

Reconstruction of Longitudinal Profiles of Ultra-High Energy Cosmic Ray Showers from Fluorescence and Cherenkov Light Measurements

M. Unger^a, B. R. Dawson^b, R. Engel^a, F. Schussler^a and R. Ulrich^a

^aInstitut für Kernphysik, Forschungszentrum Karlsruhe, Postfach 3640, 76021 Karlsruhe, Germany

^bDepartment of Physics, University of Adelaide, Adelaide 5005, Australia

Abstract

We present a new method for the reconstruction of the longitudinal profile of extensive air showers induced by ultra-high energy cosmic rays. In contrast to the typically considered shower size profile, this method employs directly the ionization energy deposit of the shower particles in the atmosphere. Due to universality of the energy spectra of electrons and positrons, both fluorescence and Cherenkov light can be used simultaneously as signal to infer the shower profile from the detected light. The method is based on an analytic least-square solution for the estimation of the shower profile from the observed light signal. Furthermore, the extrapolation of the observed part of the profile with a Gaisser-Hillas function is discussed and the total statistical uncertainty of shower parameters like total energy and shower maximum is calculated.

Key words: Cosmic rays, extensive air showers, air shower reconstruction, air fluorescence, Cherenkov light

PACS: 96.50.sd

1. Introduction

The particles of an extensive air shower excite nitrogen molecules in the atmosphere, which subsequently radiate ultraviolet fluorescence light isotropically. This fluorescence light signal can be measured with appropriate optical detectors such as the fluorescence telescopes of Hires [1], the Pierre Auger Observatory [2] or the Telescope Array [3].

The number of emitted fluorescence photons is expected to be proportional to the energy deposited by the shower particles. Recent measurements of the fluorescence yield in the laboratory confirm this expectation within the experimental uncertainties [4,5,6]. Non-radiative processes of nitrogen molecule de-excitation lead to a temperature, pressure and humidity dependence of the fluorescence yield (see e.g. [7]). For atmospheric parameters of relevance to the reconstruction of air showers of ultra-high energy cosmic rays, the pressure dependence of the ionization energy deposit per meter track length of a charged particle is almost perfectly canceled by the pressure dependence of the fluorescence yield (see, for example, [8]). Therefore only a weak pressure and temperature dependence has to be taken into account if the number of emitted photons is converted to a number of charged particle times track length, as has

been done in the pioneering Fly's Eye experiment [9]. The reconstructed longitudinal shower profile is then given by the number of charged particles as function of atmospheric depth.

The approximation of assuming a certain number of fluorescence photons per meter of charged particle track and the corresponding expression of the longitudinal shower development in terms of shower size are characterized by a number of conceptual shortcomings. Firstly the energy spectrum of particles in an air shower changes in the course of its development. A different rate of fluorescence photons per charged particle has to be assumed for early and late stages of shower development as the ionization energy deposit depends on the particle energy [10]. Secondly the tracks of low-energy particles are not parallel to the shower axis leading to another correction that has to be applied [11]. Thirdly the quantity "shower size" is not suited to a precise comparison of measurements with theoretical predictions. In air shower simulations, shower size is defined as the number of charged particles above a given energy threshold E_{cut} that cross a plane perpendicular to the shower axis. Setting this threshold very low to calculate the shower size with an accuracy of 1% leads to very large simulation times as the number of photons diverges for $E_{\text{cut}} \rightarrow 0$. Moreover, the shower size reconstructed from data depends on simulations itself since the shower size is

corresponding author, Michael.Unger@ik.fzk.de

not directly related to the fluorescence light signal.

These conceptual problems can be avoided by directly using energy deposit as the primary quantity for shower profile reconstruction as well as comparing experimental data with theoretical predictions. Due to the proportionality of the number of fluorescence photons to the energy deposit, shower simulations are not needed to reconstruct the total energy deposit at a given depth in the atmosphere. Another advantage is that the calorimetric energy of the shower is directly given by the integral of the energy deposit profile [2]. Furthermore the energy deposit profile is a well-defined quantity that can be calculated straightforwardly in Monte Carlo simulations and does not depend on the simulation threshold [13].

Most of the charged shower particles travel faster than the speed of light in air, leading to the emission of Cherenkov light. Thus, in general, the optical signal of an air shower consists of both fluorescence and Cherenkov light contributions. In the traditional method [9] for the reconstruction of the longitudinal shower development, the Cherenkov light is iteratively subtracted from the measured total light. The drawbacks of this method are the lack of convergence for events with a large amount of Cherenkov light and the difficulty of propagating the uncertainty of the subtracted signal to the reconstructed shower profile.

An alternative procedure, used in [14], is to assume a functional form for the longitudinal development of the shower, calculate the corresponding light emission and vary the parameters of the shower curve until a satisfactory agreement with the observed light at the detector is obtained. Whereas in this scheme the convergence problems of the aforementioned method are avoided, its major disadvantage is that it can only be used if the showers indeed follow the functional form assumed in the minimization.

It has been noted in [15] that, due to the universality of the energy spectra of the secondary electrons and positrons within an air shower, there exists a non-iterative solution for the reconstruction of a longitudinal shower profile from light detected by fluorescence telescopes.

Here we will present an analytic least-square solution for the estimation of the longitudinal energy deposit profile of air showers from the observed light signal, in which both fluorescence and Cherenkov light contributions are treated as signal. We will also discuss the calculation of the statistical uncertainty of the shower profile, including bin-to-bin correlations. Finally we will introduce a constrained fit to the detected shower profile for extrapolating it to the regions outside the field of view of the fluorescence telescope. This constrained fit allows us to always use the full set of profile function parameters independent of the quality of the detected shower profile.

2. Fluorescence and Cherenkov Light Signals

The non-scattered, i.e. directly observed fluorescence light emitted at a certain slant depth X_i is measured at

the detector at a time t_i . Given the fluorescence yield Y_i^f [4,16,17,5] at this point of the atmosphere, the number of photons produced at the shower in a slant depth interval X_i is

$$N^f(X_i) = Y_i^f w_i(X_i); \quad (1)$$

Here, w_i denotes the energy deposited per unit depth at slant depth X_i (cf. Fig. 1) and is defined as

$$w_i = \frac{1}{X_i} \int_0^{Z_2} \int_0^{Z_1} \int_0^Z d'r dr dz \frac{dE_{\text{dep}}}{dV}; \quad (2)$$

where $dE_{\text{dep}}=dV$ is the energy deposit per unit volume and $(r;R;z)$ are cylinder coordinates with the shower axis at $R=0$. The distance interval z_i along the shower axis is given by the slant depth interval X_i . The fluorescence yield Y_i^f is the number of photons expected per unit deposited energy for the atmospheric pressure and temperature at slant depth X_i . The photons from Eq. (1) are distributed over a sphere with surface $4\pi r_i^2$, where r_i denotes the distance of the detector. Due to atmospheric attenuation only a fraction T_i of them reach the detector aperture with area A . Given a light detection efficiency of ϵ , the measured fluorescence light flux \mathcal{Y}_i^f can be written as

$$\mathcal{Y}_i^f = d_i Y_i^f w_i(X_i); \quad (3)$$

where the abbreviation $d_i = \epsilon T_i \frac{A}{4\pi r_i^2}$ is used. For the sake of clarity the wavelength dependence of Y , T and ϵ will be disregarded in the following, but discussed later.

The number of Cherenkov photons emitted at the shower is proportional to the number of charged particles above the Cherenkov threshold energy. Since the electromagnetic component dominates the shower development, the emitted Cherenkov light, N^c , can be calculated from

$$N^c(X_i) = Y_i^c N_i^e(X_i); \quad (4)$$

where N_i^e denotes the number of electrons and positrons above a certain energy cutoff, which is constant over the full shower track and not to be confused with the Cherenkov emission energy threshold. Details of the Cherenkov light production like these thresholds are included in the Cherenkov yield factor Y_i^c [15,18,19,20].

Although Cherenkov photons are emitted in a narrow cone along the particle direction, they cover a considerable angular range with respect to the shower axis, because the charged particles are deflected from the primary particle direction due to multiple scattering. Given the fraction $f_c(\theta_i)$ of Cherenkov photons per solid angle emitted at an angle θ_i with respect to the shower axis [18,20], the light flux at the detector aperture originating from direct Cherenkov light is

$$\mathcal{Y}_i^c = d_i f_c(\theta_i) Y_i^c X_i N_i^e; \quad (5)$$

Due to the forward peaked nature of Cherenkov light production, an intense Cherenkov light beam builds up along the shower as it traverses the atmosphere (cf. Fig. 1). If a fraction $f_s(\theta_i)$ of the beam is scattered towards the observer it can contribute significantly to the total light received at the detector. In a simple one-dimensional model

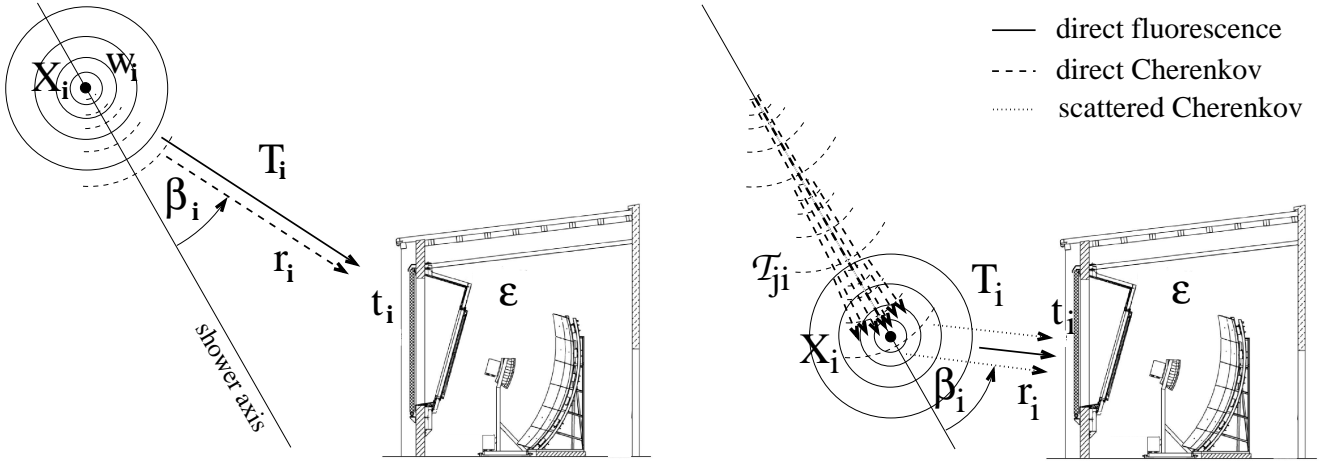


Fig. 1. Illustration of the isotropic fluorescence light emission (solid circles), Cherenkov beam along the shower axis (dashed arcs) and the direct (dashed lines) and scattered (dotted lines) Cherenkov light contributions.

the number of photons in the beam at depth X_i is just the sum of Cherenkov light produced at all previous depths X_j attenuated on the way from X_j to X_i by T_{ji} :

$$N^{\text{beam}}(X_i) = \sum_{j=0}^{X_i} T_{ji} Y_j^C X_j N_j^e \quad (6)$$

Similar to the direct contributions, the scattered Cherenkov light received at the detector is then

$$Y_i^{Cs} = d_i f_s(\beta_i) \sum_{j=0}^{X_i} T_{ji} Y_j^C X_j N_j^e \quad (7)$$

Finally, the total light received at the detector at the time t_i is obtained by adding the scattered and direct light contributions:

$$Y_i = Y_i^f + Y_i^{Cd} + Y_i^{Cs} \quad (8)$$

3. Analytic Shower Profile Reconstruction

The aim of the profile reconstruction is to estimate the energy deposit and/or electron profile from the light flux observed at the detector. At first glance this seems to be hopeless, since at each depth there are the two unknown variables w_i and N_i^e , and only one measured quantity, namely y_i . Since the total energy deposit is just the sum of the energy loss of electrons, w_i and N_i^e are related via

$$w_i = N_i^e \int_0^{Z_1} f_e(E; X_i) w_e(E) dE \quad (9)$$

where $f_e(E; X_i)$ denotes the normalized electron energy distribution and $w_e(E)$ is the energy loss per unit depth of a single electron with energy E . As is shown in [15,19,20], the electron energy spectrum $f_e(E; X_i)$ is universal in shower age $s_i = 3 = (1 + 2X_{\text{max}}/X_i)$, i.e. it does not depend on the primary mass or energy, but only on the relative distance to the shower maximum, X_{max} . Eq. (9) can thus be simplified to

$$w_i = N_i^e \alpha_i \quad (10)$$

where α_i is the average energy deposit per unit depth per electron at shower age s_i . Parameterizations of α_i can be found in [10,20]. With this one-to-one relation (Eq. 10) between the energy deposit and the number of electrons, the shower profile is readily calculable from the equations given in the last section. For the solution of the problem, it is convenient to rewrite the relation between energy deposit and light at the detector in matrix notation: Let $y = (y_1; y_2; \dots; y_n)^T$ be the n -component vector (histogram) of the measured photon flux at the aperture and $w = (w_1; w_2; \dots; w_n)^T$ the energy deposit vector at the shower track. Using the expression

$$y = C w \quad (11)$$

the elements of the Cherenkov-fluorescence matrix C can be found by a comparison with the coefficients in equations (3), (5) and (7):

$$C_{ij} = \begin{cases} \geq 0; & i < j \\ C_i^d + C_{ji}^s; & i = j \\ C_{ij}^s; & i > j; \end{cases} \quad (12)$$

where

$$C_i^d = d_i Y_i^f + f_c(\beta_i) Y_i^C = \alpha_i X_i \quad (13)$$

and

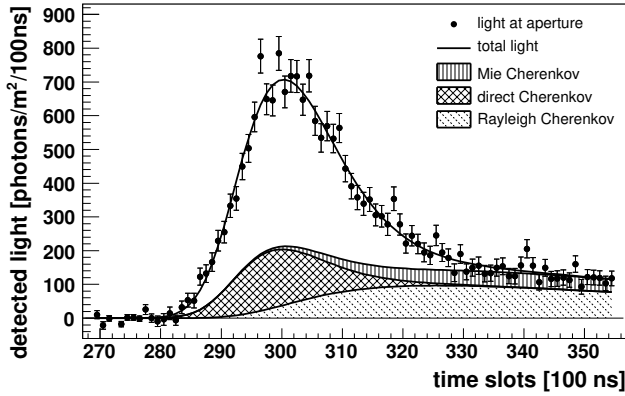
$$C_{ij}^s = d_i f_s(\beta_i) T_{ji} Y_j^C = \alpha_j X_j \quad (14)$$

The solution of Eq. (11) can be obtained by inversion, leading to the energy deposit estimator \hat{w} :

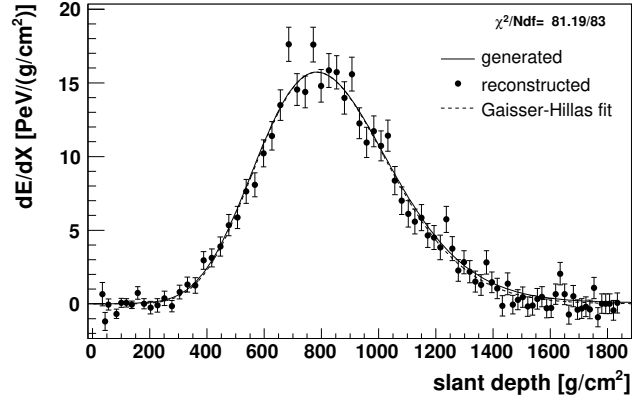
$$\hat{w} = C^{-1} y \quad (15)$$

Due to the triangular structure of the Cherenkov-fluorescence matrix the inverse can be calculated quickly even for matrices with large dimension. As the matrix elements in Eq. (12) are always ≥ 0 , C is never singular. The statistical uncertainties of \hat{w} are obtained by error propagation:

$$V_w = C^{-1} V_y C^{-T} \quad (16)$$



(a) Light at aperture.



(b) Energy deposit profile

Fig. 2. Example of a simulated 10^{19} eV proton shower.

It is interesting to note that even if the measurements y_i are uncorrelated, i.e. their covariance matrix V_y is diagonal, the calculated energy loss values w_i are not. This is because the light observed during time interval i does not solely originate from w_i , but also receives a contribution from earlier shower parts w_j , $j < i$, via the Cherenkov light beam.

4. Wavelength Dependence

Until now it has been assumed that the shower induces light emission at a single wavelength. In reality, the fluorescence yield shows distinct emission peaks and the number of Cherenkov photons produced is proportional to $\frac{1}{\lambda^2}$. In addition the wavelength dependence of the detector efficiency and the light transmission need to be taken into account. Assuming that a binned wavelength distribution of the yields is available ($Y_{ik} = \sum_k R_{k+} Y_i(\lambda_k)$), the above considerations still hold when replacing c_i^d and c_{ij}^s in Eq. (12) by

$$c_i^d = \sum_k X_i d_{ik} Y_{ik}^f + f_c(\lambda_i) Y_{ik}^c = i \quad (17)$$

and

$$c_{ij}^s = \sum_k X_j d_{ik} f_s(\lambda_i) T_{jik} Y_{jk}^c = j; \quad (18)$$

where

$$d_{ik} = \frac{\mu_k T_{ik}}{4 r_i^2}; \quad (19)$$

The detector efficiency μ_k and transmission coefficients T_{ik} and T_{jik} are evaluated at the wavelength λ_k .

5. Validation with Air Shower Simulations

In order to test the performance of the reconstruction algorithm we will use in the following simulated fluorescence detector data. For this purpose we generated proton air showers with an energy of 10^{19} eV with the CONEX [21]

event generator. The resulting longitudinal charged particle and energy deposit profiles were subsequently fed into the atmosphere and detector simulation package [22] of the Pierre Auger Observatory. The geometry and profile of the events in this simulated data sample was then reconstructed within the Auger online software framework [23].

Only events satisfying basic quality selection criteria have been used in the analysis. In order to assure a good reconstruction of the shower geometry, the angular length of the shower in age on the camera was required to be larger than nine degrees. Moreover, we only selected events with at least one coincident surface detector tank (so-called hybrid geometry reconstruction [24]). Furthermore we rejected under-determined measured longitudinal profiles by demanding an observed slant depth length of $> 300 \text{ g cm}^{-2}$ and a reconstructed shower maximum within the field of view of the detector.

An example of a simulated event is shown in Fig. 2, illustrating that the shape of the light curve at the detector can differ considerably from the one of the energy deposit profile due to the scattered Cherenkov light detected at late stages of the shower development. The reconstructed energy deposit curve, however, shows on average a good agreement with the generated profile.

Since longitudinal air shower profiles exhibit similar shapes when transformed from slant depth X to shower age s (see for instance [25]), a good test of the profile reconstruction performance is to compare the average generated and reconstructed energy deposit profiles as a function of s normalized to the energy deposit at shower maximum. As can be seen in Fig. (3), the difference between these averages is 1.5% and it can be concluded that the matrix method introduced here performs well in reconstructing air shower profiles without a prior assumption about their functional shape.

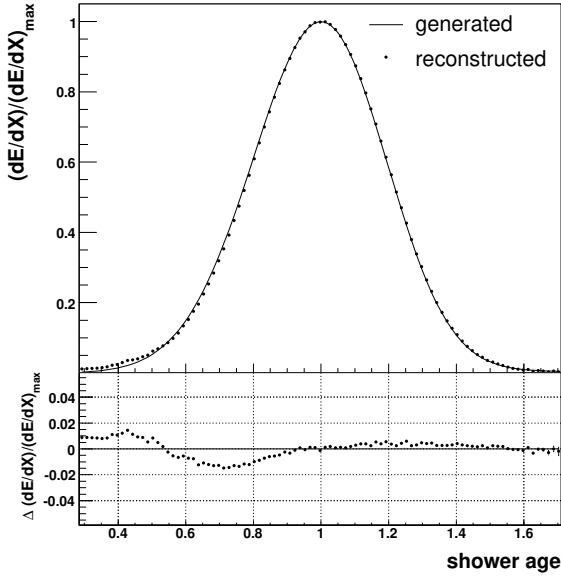


Fig. 3. Average generated and reconstructed energy deposit profiles.

6. Shower Age Dependence

Due to the age dependence of the electron spectra $f_e(E; s_i)$, the Cherenkov yield factors Y_i^C and the average electron energy deposits ϵ_i depend on the depth of shower maximum, which is not known before the profile has been reconstructed. Fortunately, these dependencies are small: In the age range of importance for the shower profile reconstruction (s 2 [0.8; 1.2]) ϵ_i varies by only a few percent [20] and Y_i^C by less than 15% [15]. Therefore, a good estimate of ϵ_i and Y_i^C can be obtained by setting $s = 1$ over the full profile or by estimating X_{max} from the position maximum of the detected light profile. After the shower profile has been calculated with these estimates, X_{max} can be determined from the energy deposit profile and the profile can be re-calculated with an updated Cherenkov-corescence matrix. The convergence of this procedure is shown in Fig. 5. After only one iteration the X_{max} (energy) differs by less than 0.1 g cm^{-2} (0.1%) from its asymptotic value. Note that age dependent effects of the lateral spread of the shower on the image seen at the detector [26,27], though not discussed in detail here, have also been included in the simulation and reconstruction.

7. Gaisser-Hillas Fit

A knowledge of the complete profile is required for the calculation of the Cherenkov beam and the shower energy. If due to the limited field of view of the detector only a part of the profile is observed, an appropriate function for the extrapolation to unobserved depths is needed. A possible choice is the Gaisser-Hillas function [28]

$$f_{GH}(X) = w_{max} \frac{X - X_0}{X_{max} - X_0} e^{-(X_{max} - X_0) \frac{X - X_0}{X_{max} - X_0}}; \quad (20)$$

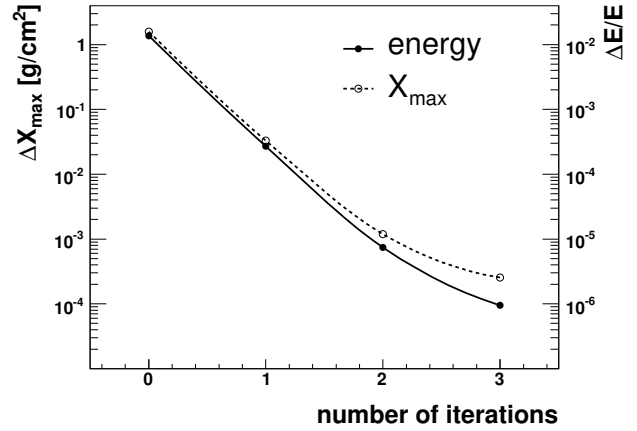


Fig. 5. X_{max} and energy difference with respect to the tenth shower age iteration.

which was found to give a good description of measured longitudinal profiles [29]. It has four free parameters: X_{max} , the depth where the shower reaches its maximum energy deposit w_{max} and two shape parameters X_0 and σ . The best set of Gaisser-Hillas parameters p can be obtained by minimizing the error weighted squared difference between the vector of function values f_{GH} and \mathbf{w} , which is

$$\chi_{GH}^2 = [\mathbf{w} - f(p)]^T V_w^{-1} [\mathbf{w} - f(p)]; \quad (21)$$

This minimization works well if a large fraction of the shower has been observed below and above the shower maximum. If this is not the case, or even worse, if the shower maximum is outside the field of view, the problem is underdetermined, i.e. the experimental information is not sufficient to reconstruct all four Gaisser-Hillas parameters. This complication can be overcome by constraining X_0 and σ to their average values $\langle X_0 \rangle$ and $\langle \sigma \rangle$. The new minimization function is then the modified χ^2

$$\chi^2 = \chi_{GH}^2 + \frac{(X_0 - \langle X_0 \rangle)^2}{V_{X_0}} + \frac{(\sigma - \langle \sigma \rangle)^2}{V}; \quad (22)$$

where the variances of X_0 and σ around their mean values are in the denominators.

In this way, even if χ_{GH}^2 is not sensitive to X_0 and σ , the minimization will still converge. On the other hand, if the measurements have small statistical uncertainties and/or cover a wide range in depth, the minimization function is flexible enough to allow for shape parameters differing from their mean values. These mean values can be determined from air shower simulations or, preferably, from high quality data profiles which can be reconstructed without constraints.

Eq. (22) can be easily extended to incorporate correlations between X_0 and σ and the energy dependence of their mean values. Air shower simulations indicate a small logarithmic energy dependence of the latter ($\sim 25\%$ and 5% per decade for X_0 and σ respectively [30]). In practice it is sufficient to use energy independent values determined at low energies, because at high energies the number of measured points

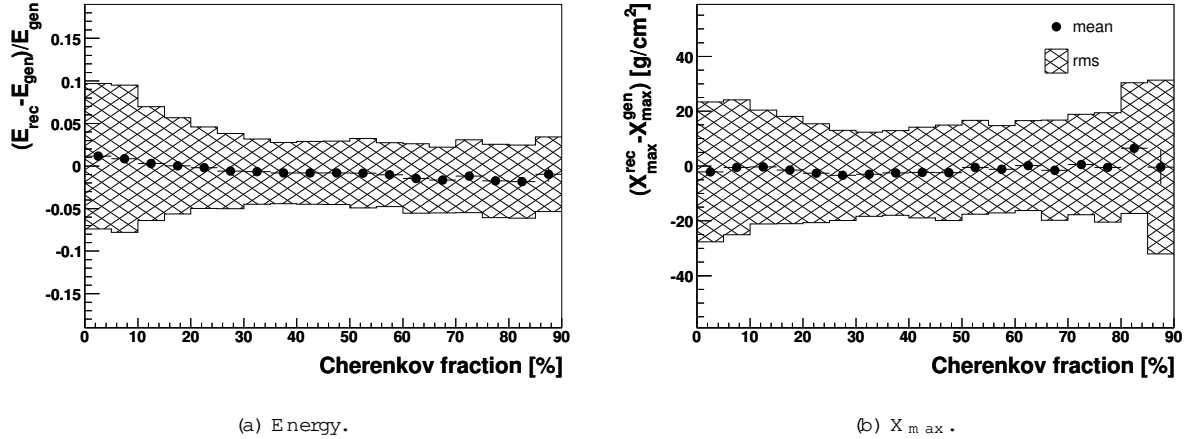


Fig. 4. Energy and X_{\max} reconstruction accuracy as function of the amount of detected Cherenkov light.

is large and thus the constraints do not contribute significantly to the overall σ^2 .

The accuracy of the reconstructed energy, obtained by integrating over the Gaisser-Hillas function (see below), and that of the depth of shower maximum, are displayed in Fig. 4 as a function of the relative amount of Cherenkov light. Note that the good resolutions of 7% and 20 g/cm² are of course not a feature of the reconstruction method alone, but depend strongly on the detector performance and quality selection. The mean values of difference to the true shower parameters, however, which are close to zero for both fluorescence and Cherenkov light dominated events, indicate that both light sources are equally suited to reconstruct the longitudinal development of air showers.

A slight deterioration of the resolutions can be seen for events with a very small Cherenkov contribution of < 10%. Such showers are either inclined events which developed high in the atmosphere where the light scattering probabilities are low or deep vertical showers, for which most of the late part of the shower is below ground level. Both topologies result in a somewhat worse resolution: The former correspond to larger than average distances to the detector and the latter to shorter observed profiles.

8. Error Propagation

A realistic estimate of the statistical uncertainties of important shower parameters is desired for many purposes, like data quality selection cuts, or the comparison between independent measurements like the surface and fluorescence detector measurements of the Pierre Auger Observatory or the Telescope Array. The uncertainties of w_{\max} , X_{\max} , X_0 and β obtained after their minimization of Eq. (22), reflect only the statistical uncertainty of the light flux, which is why these errors will be referred to as 'flux uncertainties' (σ_{flux}) in the following. Additional uncertainties arise from the uncertainties on the shower geometry (σ_{geo}), atmosphere (σ_{atm}) and the correction for invisible energy (σ_{inv}).

8.1. Flux uncertainty of the calorimetric energy

Even with the flux uncertainties of the Gaisser-Hillas parameters it is not straightforward to calculate the flux uncertainty of the calorimetric energy, which is given by the integral over the energy deposit profile:

$$E_{\text{cal}} = \int_0^{Z_1} f_{\text{GH}}(X) dX \quad (23)$$

To solve this integral one can substitute

$$t = \frac{X - X_0}{\beta} \quad \text{and} \quad \beta = \frac{X_{\max} - X_0}{\beta} \quad (24)$$

in the Gaisser-Hillas function Eq. (20) to get

$$f_{\text{GH}}(t) = w_{\max} \frac{e^{-t}}{\beta} e^{-t}; \quad (25)$$

which can be identified with a Gamma distribution. Therefore, the above integral is given by

$$E_{\text{cal}} = w_{\max} \frac{e^{-t}}{\beta} (\beta + 1); \quad (26)$$

where Γ denotes the Gamma-function. Thus, instead of doing a tedious error propagation to determine the statistical uncertainty of E_{cal} one can simply use it directly as a free parameter in the fit instead of the conventional factor w_{\max} :

$$f_{\text{GH}}(t) = \frac{E_{\text{cal}}}{(\beta + 1)} e^{-t} \quad (27)$$

In this way, $\sigma_{\text{flux}}(E_{\text{cal}})$ is obtained directly from the $\beta + 1$ contour of Eq. (22).

8.2. Geometric uncertainties

Due to the uncertainties on the shower geometry, the distances r_i to each shower point are only known within a limited precision and correspondingly the energy deposit profile points are uncertain due to the transmission factors $T(r_i)$ and geometry factors $1 = (4 - r_1^2)$. Furthermore, the uncertainty of the shower direction, especially

the zenith angle θ , affects the slant depth calculation via $X_{\text{slant}} = X_{\text{vert}} / \cos \theta$ and thus X_{max} . Finally, the amount of direct and scattered Cherenkov light depends on the shower geometry, too, via the angles θ_i .

The algorithms used to reconstruct the shower geometry from fluorescence detector data usually determine the following five parameters Ψ , irrespective of whether the detectors operate in monocular, stereo or hybrid mode:

$$\Psi = \{ \theta_{\text{SDP}}; \phi_{\text{SDP}}; T_0; R_p; \sigma_0 \} \quad (28)$$

θ_{SDP} and ϕ_{SDP} are the angles of the normal vector of a plane spanned by the shower axis and the detector (the so called shower-detector-plane), θ_0 denotes the angle of the shower within this plane and T_0 and R_p are the time and distance of the shower at its point of closest approach to the detector.

For any function $q(\Psi)$ standard error propagation yields the geometric uncertainty

$$\sigma_{\text{geom}}^2(q) = \sum_{i=1}^5 \sum_{j=1}^5 \frac{dq}{d\Psi_i} \frac{dq}{d\Psi_j} V_{ij}; \quad (29)$$

where V denotes the covariance matrix of the axis parameters. As the calorimetric energy and X_{max} depend non-trivially on the shower geometry, the above derivatives need to be calculated numerically, i.e. by repeating the profile reconstruction and Gaisser-Hillas fitting for the ten new geometries given by $\Psi_i \pm \frac{V_{ii}}{V_{ii}}$ to obtain

$$\frac{dq}{d\Psi_i} = \frac{1}{2} [q(\Psi_i + \frac{V_{ii}}{V_{ii}}) - q(\Psi_i - \frac{V_{ii}}{V_{ii}})]; \quad (30)$$

with which Eq. (29) reads as

$$\sigma_{\text{geom}}^2(q) = \sum_{i=1}^5 \sum_{j=1}^5 \frac{dq}{d\Psi_i} \frac{dq}{d\Psi_j} V_{ij} \quad (31)$$

where

$$\rho_{ij} = \frac{V_{ij}}{\sqrt{V_{ii} V_{jj}}} \quad (32)$$

denote the correlation coefficients of the geometry parameters Ψ_i and Ψ_j .

8.3. Atmospheric uncertainties

Whereas the Rayleigh attenuation is a theoretically well understood process, the molecular density profiles and aerosol content of the atmosphere vary due to environmental influences and need to be well monitored in order to determine the slant depth and transmission coefficients needed for the profile reconstruction. Uncertainties in these measured atmospheric properties (see for instance [31,32]) can be propagated in the same way as the geometric uncertainties by determining the one sigma shower parameter deviations via Eq. (30).

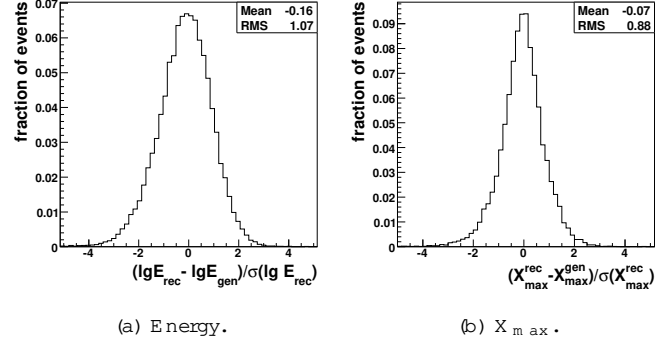


Fig. 6. Pull distributions

8.4. Invisible energy

Not all of the energy of a primary cosmic ray particle ends up in the electromagnetic part of an air shower. Neutrinos escape undetected and muons need long path lengths to fully release their energy. This is usually accounted for by multiplying the calorimetric energy, Eq. (23), with a correction factor f_{inv} determined from shower simulations to obtain the total primary energy

$$E_{\text{tot}} = f_{\text{inv}} E_{\text{cal}}; \quad (33)$$

The meson decay probabilities, and thus the amount of neutrino and muon production, decrease with energy, therefore f_{inv} depends on the primary energy. For instance, in [33] it is parameterized as

$$f_{\text{inv}} = (a + b E_{\text{cal}}^c)^{-1}; \quad (34)$$

where a , b and c denote constants depending on the primary composition and interaction model assumed¹. This energy dependence needs to be taken into account when propagating the calorimetric energy uncertainty to the total energy uncertainty.

Due to the stochastic nature of air showers, the correction factor is subject to shower-to-shower fluctuations. The statistical uncertainty of f_{inv} was determined in [34] and can be parameterized as follows:

$$(f_{\text{inv}})_{\text{stat}} = 1.663 \cdot 10^{-3} \cdot \lg(E_{\text{tot}} / \text{eV})^{6.36}; \quad (35)$$

Typical values are 2.5% at 10^{17} eV and 0.9% at 10^{20} eV.

8.5. Total statistical uncertainty

Summarizing the above considerations, the statistical variance of the total energy is

$$\sigma_{\text{stat}}^2(E_{\text{tot}}) = E_{\text{tot}}^2 \left[\sigma_{\text{geom}}^2 + \left(\frac{df_{\text{inv}}}{dE_{\text{cal}}} E_{\text{cal}} + f_{\text{inv}} \right)^2 \sum_i \sigma_i^2(E_{\text{cal}}) \right]; \quad (36)$$

¹ Note that here only the statistical uncertainties of the invisible energy correction are discussed. For an estimate on the related systematic uncertainties see [34]

where i runs over the geometric, atmospheric and flux uncertainties. Since the invisible energy correction does not affect the depth of shower maximum, its uncertainty is simply given by

$$\sigma_{\text{stat}}(X_{\text{max}}) = \frac{\sigma_X}{X} \sqrt{\sum_i \sigma_i^2(X_{\text{max}})} : \quad (37)$$

Again we use simulated events to verify the validity of the above considerations. The pull distributions of the reconstructed energy and shower maximum, shown in Fig. 37, both have a width of approximately one, which means that the total uncertainties from Eqs. (36) and (37) are good estimators for the actual event-by-event measurement uncertainties.

9. Conclusions and Outlook

In this paper a new method for the reconstruction of longitudinal air shower profiles was presented. With the help of simulations we have shown that the least square solution yields robust and unbiased results and that uncertainties of shower parameters can be reliably calculated for each event.

Events with a large Cherenkov light contribution are currently usually rejected during the data analysis (see for instance [14,35]) However, as we have shown, there is no justification for rejecting such showers, once experimental systematic uncertainties are well understood. Because events with a large Cherenkov contribution have different systematic uncertainties to those dominated by fluorescence light, both event classes can be compared to study their compatibility.

At energies below $10^{17.5}$ eV, where new projects [36,37] are planned to study the transition from galactic to extragalactic cosmic rays, events with a large fraction of direct Cherenkov light will dominate the data samples, because the amount of light, and thus trigger probability, of these events is much larger than that of a fluorescence dominated shower. If at these energies it is still possible to measure an accurate shower geometry, the fluorescence detectors should in fact be used as Cherenkov-Fluorescence telescopes.

Acknowledgments The authors would like to thank their colleagues from the Pierre Auger Collaboration, in particular Frank Nerling and Tanguy Pierog, for fruitful discussions.

References

- [1] T. Abu-Zayyad et al. [HiRes Collaboration], Nucl. Instrum. Meth. A 450 (2000) 253.
- [2] J. Abraham et al. [Pierre Auger Collaboration], Nucl. Instrum. Meth. A 523 (2004) 50.
- [3] H. Kawai et al. [TA Collaboration], Proc. 29th ICRC (2005).
- [4] F. Kakimoto et al., Nucl. Instrum. Meth. A 372 (1996) 527.
- [5] T. Walkdenmaier, J. Blümer, H. Kages, astro-ph/0709.1494.
- [6] M. Ave et al. [IRFLY Collaboration], Proc. 30th ICRC (2007) and arXiv:0711.4519 [astro-ph].
- [7] P. Privitera et al. [IRFLY Collaboration], Proc. 30th ICRC (2007).
- [8] B. Keilhauer, J. Blümer, R. Engel, H. O. Kages, Astropart. Phys. 25 (2006) 259.
- [9] R.M. Baltrusaitis et al. [Fly's Eye Collaboration], Nucl. Instrum. Meth. A 240 (1985) 410.
- [10] C. Song et al., Astropart. Phys. 14 (2000) 7.
- [11] J. Alvarez-Muniz, E. Marques, R. A. Vazquez, E. Zas, Phys. Rev. D 67 (2003) 101303.
- [12] J. Lindsley, Proc. 27th ICRC (2001).
- [13] M. Risse, D. Heck, Astropart. Phys. 20 (2004) 661.
- [14] R. U. Abbasi et al. [HiRes Collaboration], Astrophys. J. 622 (2005) 910.
- [15] M. Giller et al., J. Phys. G 30 (2004) 97.
- [16] M. Nagano et al., Astropart. Phys. 22 (2004) 235.
- [17] M. Ave et al. [IRFLY Collaboration], Astropart. Phys. 28 (2007) 41.
- [18] A.M. Hillas, J. Phys. G 8 (1982) 1461.
- [19] A.M. Hillas, J. Phys. G 8 (1982) 1475.
- [20] F. Nerling et al., Astropart. Phys. 24 (2006) 421.
- [21] T. Bergmann et al., Astropart. Phys. 26 (2007) 420.
- [22] L. Pardo et al., Nucl. Instrum. Meth. A 545 (2005) 632.
- [23] S. A. R. G. et al., Nucl. Instrum. Meth. A 580 (2007) 1485.
- [24] P. Sommers, Astropart. Phys. 3 (1995) 349.
- [25] M. Giller et al., J. Phys. G 31 (2005) 947.
- [26] D. Gora et al., Astropart. Phys. 24 (2006) 484.
- [27] M. Giller et al., Astropart. Phys. 18 (2003) 513.
- [28] T. K. Gaisser, A.M. Hillas, Proc. 15th ICRC (1977).
- [29] Z. Cao et al., Proc. 28th ICRC (2003).
- [30] L. Perrone, INFN Lecce, private communication.
- [31] S. Y. BenZvi et al. [Pierre Auger Collaboration], Proc. 30th ICRC (2007), astro-ph/0706.3236.
- [32] B. Keilhauer et al. [Pierre Auger Collaboration], Proc. 29th ICRC (2005), astro-ph/0507275.
- [33] H.M.J. Barbosa et al., Astropart. Phys. 22 (2004) 159.
- [34] T. Pierog et al., Proc. 29th ICRC (2005).
- [35] T. Abu-Zayyad et al. [HiRes/Mia Collaboration], Astrophys. J. 557 (2001) 686.
- [36] H. Kages et al. [Pierre Auger Collaboration], Proc. 30th ICRC (2007).
- [37] J. Belz et al. [TA/TALE Collaboration], Proc. 30th ICRC (2007).